Trends in Chemistry

CellPress

Review

Deciphering plasmonic photocatalysis using plasmon-enhanced Raman spectroscopy

Hui Wang [1,*]

Plasmonic photocatalysis, which represents a paradigm-shifting approach to solar-to-chemical energy conversion, has become a rapidly evolving research field full of opportunities, challenges, and open questions. Plasmon-driven photocatalytic reactions are mechanistically complex, dictated not only by multiple interplaying photophysical effects but also by local chemical environments at the catalyst–adsorbate interfaces. This review article highlights the unique value of plasmon-enhanced Raman spectroscopy in mechanistic studies of plasmonic photocatalysis. Using plasmon-driven reductive coupling of nitroarene derivative adsorbates as a model reaction system, this article elaborates on how the rich information extracted from deliberately designed plasmon-enhanced Raman spectroscopic measurements can be carefully analyzed and further rationalized to generate critical insights into the exact roles of hot carriers, photothermal transduction, and catalyst–adsorbate interactions in plasmonic photocatalysis.

Highlights

Plasmon-enhanced Raman scattering provides an *in situ* spectroscopic tool, particularly useful for mechanistic studies of plasmonic photocatalysis.

Time-resolved surface-enhanced Raman scattering (SERS)/tip-enhanced Raman scattering (TERS) provides critical information about dynamic molecular behaviors and the underlying hot carrier transfer pathways involved in plasmonic photocatalysis.

Local temperatures at the photocatalytically active sites in plasmonic hot spots can be measured by SERS/TERS-based nanothermometry, enabling quantification of thermal and nonthermal contributions in plasmonic photocatalysis.

Detailed molecular fingerprinting and kinetic information extracted from SERS/TERS shed light on the relationships between the chemical nature of metal–adsorbate interactions and plasmonic reactivity of molecular adsorbates.

Plasmonic photocatalysis: a paradigm-shift in heterogeneous photocatalysis

Metallic nanostructures have emerged as a class of subwavelength optical components that interact strongly with incident light through resonant excitations of free electron oscillations, known as plasmons. The plasmonic electron oscillations decay radiatively through photon scattering, which results in large local-field enhancements near the nanostructure surfaces, or nonradiatively through **Landau damping** (see Glossary), in which highly energetic electrons and holes are created within 1–100 fs (Figure 1A) [1,2]. These photoexcited electrons and holes are termed 'hot' carriers because their energy distribution profiles are far from thermal equilibrium. Immediately following Landau damping, the photoexcited hot electrons undergo a carrier relaxation process, typically within 100 fs to 1 ps, to redistribute their energies via electron–electron scattering, approaching an incoherent **Fermi–Dirac distribution** of hot carriers at an elevated effective electron temperature. The relaxed hot electrons then interact with phonons and become thermalized over a timescale of 100 ps to 10 ns, which causes temperature elevation in the material lattices followed by dissipation of heat to the surroundings. The aforementioned plasmonic photophysical effects can all be judiciously harnessed to drive or enhance intriguing chemical transformations of molecular adsorbates on metal surfaces along unique pathways inaccessible by catalytic reactions under thermal conditions [3–8]. Plasmonic photocatalysts also differ strikingly from their conventional semiconductor counterparts in terms of photoexcitation mechanisms, charge carrier properties, catalyst–adsorbate interactions, excitation power-dependency of reaction rates, and molecule-transforming pathways [5,9,10]. Therefore, plasmonic photocatalysis represents a paradigm shift in heterogenous photocatalysis, creating unique pathways for solar-to-chemical energy conversion. Recent progress in plasmonic photocatalysis has been documented by a series of comprehensive review articles, which broadly cover various critical aspects concerning energetics and dynamics of hot carriers [1,8,11–13], materials design principles [7,14,15], *in situ* spectroscopic/microscopic techniques for mechanistic studies [16–18], and important

[1]Department of Chemistry and Biochemistry, University of South Carolina, Columbia, SC 29208, USA

*Correspondence: wang344@mailbox.sc.edu (H. Wang).

chemical conversions directly relevant to clean energy and sustainability [19–21], such as CO_2 reduction, water splitting, and N_2 fixation. Controversial issues, open questions, and key challenges in this research area have also been discussed by several thought-provoking perspective articles [22–24].

The past decade has witnessed discoveries of a continuously expanding library of plasmon-mediated photocatalytic reactions ranging from bond-cleaving molecular scissoring to bond-forming coupling and polymerization reactions [3–5,8]. However, it often remains challenging to fully elucidate the detailed reaction mechanisms. Local-field enhancements, hot carriers, and photothermal transduction can all play crucial roles, either individually or synergistically, in plasmon-mediated photocatalytic processes. When resonant with the plasmons in metallic nanostructures, vibronic transitions in molecular adsorbates can be drastically enhanced due to large local-field enhancements (Figure 1B), promoting the production of reactive species populating the excited vibronic states [6,25,26]. Another key mechanism for plasmonic photocatalysis involves formation of transient anionic intermediates through either indirect metal-to-adsorbate transfer of hot electrons following Landau damping (Figure 1C) [6,27] or direct excitation of electrons in an unoccupied adsorbate orbital through **chemical interface damping (CID)** (Figure 1D) [6,28,29]. Both intramolecular excitation and hot electron injection can significantly reduce the activation energy barriers for bond cleavage as the excited adsorbate molecules may either evolve along the potential energy surface of the excited electronic state or relax to excited vibrational states in the ground electronic state (Figure 1E,F). It is noteworthy that plasmonic hot holes can also be harnessed to drive photochemical transformations upon transfer of electrons from molecular adsorbates to metallic nanostructures (Figure 1C). Photothermal heating at metal–adsorbate interfaces enables deposition of thermal energy into bond vibrations in molecular adsorbates (Figure 1G), offering an additional mechanism for kinetic enhancements [6]. There is an urgent need to develop thorough understanding of detailed reaction mechanisms from both photophysical and photochemical perspectives, which will lay a solid foundation for rational optimization of plasmon-driven photocatalytic molecule-transforming processes.

Plasmon-enhanced Raman spectroscopy: a powerful tool for mechanistic studies

When a molecular adsorbate resides in a hot spot on the surface of an optically excited plasmonic nanostructure, its inelastic scattering signals can be dramatically amplified by multiple orders of magnitude, an interesting phenomenon known as surface-enhanced Raman scattering (SERS) [30,31]. The amplification of Raman signals is intimately tied to the local-field enhancements at the metal–adsorbate interfaces [32], even approaching the single-molecule detection sensitivity in certain hot spots [33]. Besides the electromagnetic enhancements, charge transfer between molecular adsorbates and metallic substrates may provide additional contributions to the overall Raman enhancements, an effect known as chemical enhancement of SERS [31]. The most widely adopted strategies for constructing plasmonic hot spots exploitable for SERS involve either creation of nanoscale interparticle gaps in deliberately assembled multi-nanoparticle systems [34] or introduction of sharply curved surface features to individual metallic nanoparticles [35–37]. An alternative way to create hot spots involves placement of a metallic tip near a metal surface to assemble tip-adsorbate-substrate junctions, a spectroscopic technique known as tip-enhanced Raman scattering (TERS) [38]. Benefiting from a unique combination of its surface-sensitivity, time-resolving capability, and molecular fingerprinting function, plasmon-enhanced Raman spectroscopy, including both SERS and TERS, has become not only an exploratory tool for discovering new plasmon-driven reactions, but also an *in situ* spectroscopic tool for fine-resolving dynamic molecule-transforming behaviors during plasmon-mediated photocatalytic reactions [17,39–41].

Glossary

Chemical interface damping (CID): plasmon damping caused by chemical species adsorbed on metallic nanostructure surfaces. In plasmonic photocatalysis, CID typically involves direct excitation of an electron in an unpopulated orbital of a strongly coupled metal–adsorbate system, which avoids the intermediate creation of hot electrons in the metals.

Fano resonance: a type of resonant scattering phenomenon signified by an asymmetric spectral line-shape. The Fano resonance line-shape results from the interference between two scattering amplitudes, one due to scattering within a continuum of states and the other due to a resonant excitation of a discrete state.

Fermi–Dirac distribution: the energy distribution of indistinguishable Fermions at thermodynamic equilibrium. The number of fermions in the *ith* energy state (n_i) is related to temperature (T), energy of the state (E_i), and total chemical potential (μ) through the following equation:

$$n_i = \frac{1}{\exp\left(\frac{E_i - \mu}{k_B T}\right) + 1} \quad [I]$$

where k_B is the Boltzmann constant.

Landau damping: a quantum mechanical process, in which the energy of an incident photon is absorbed by a metallic nanostructure to excite a single electron–hole pair within the conduction band over a timescale ranging from 1 to 100 fs.

π-Back donation: some molecular adsorbates covalently interact with the metal surface though π-back donation, which involves electron back donation from the valence band of the metal to an antibonding π* orbital of the adsorbates.

σ-Donation: in the context of chemisorption of molecular adsorbates to a metal surface, σ-donation refers to the donation of lone-pair electrons in the molecular adsorbates to the conduction band of the metal, which forms σ-type covalent interactions between the molecule and the metal.

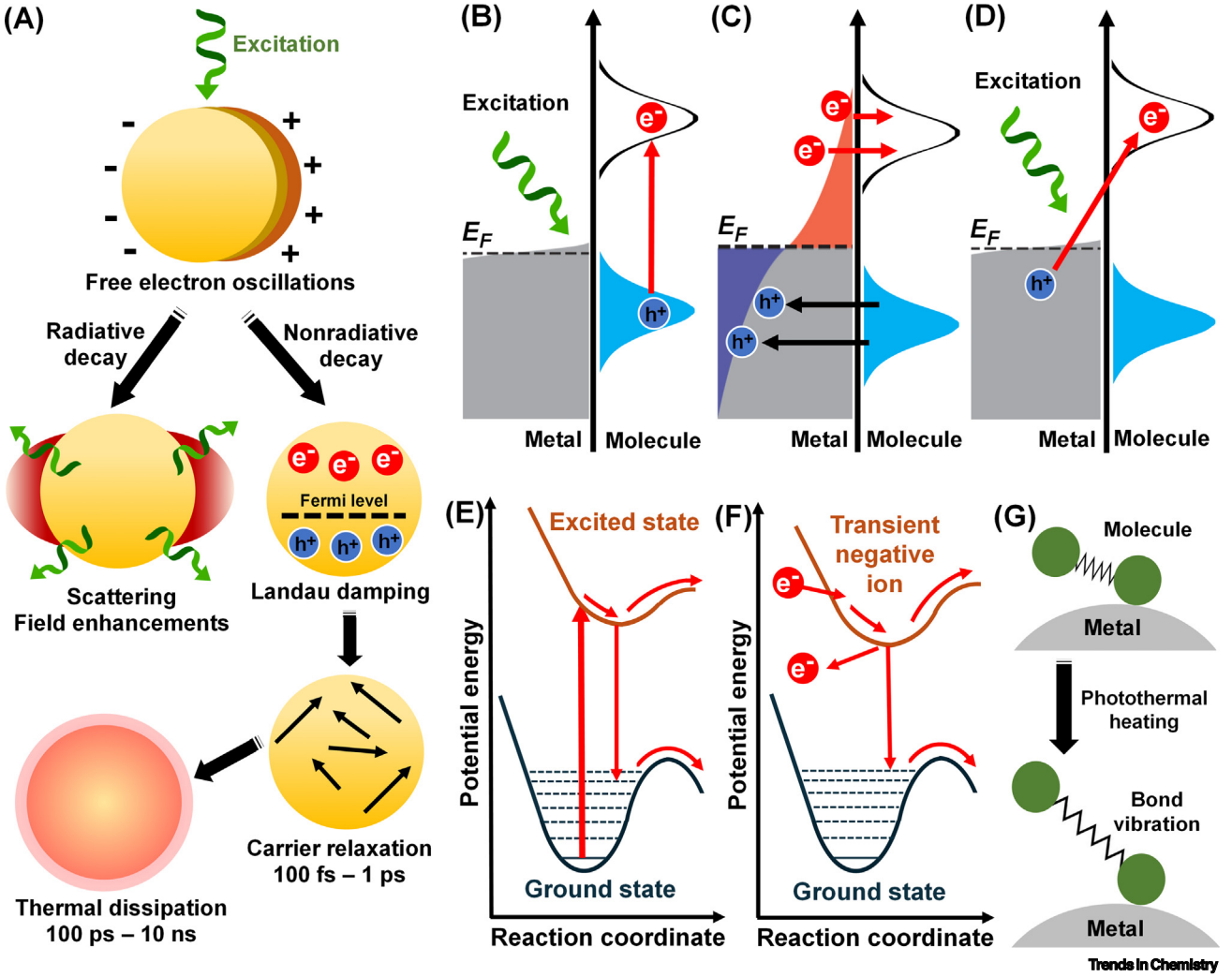

Figure 1. Mechanisms of plasmonic photocatalysis. (A) Schematic illustration of optical excitation, radiative decay, and nonradiative decay (Landau damping) of plasmon resonances in a metal nanoparticle. Schematic illustrations of (B) plasmon-enhanced intramolecular electronic excitations, (C) indirect hot carrier transfer following Landau damping, and (D) direct electron injection in molecular adsorbates through chemical interface damping. Potential energy surfaces for a photocatalytic reaction driven by (E) intramolecular electronic excitation and (F) hot electron injection. (G) Schematic illustration of a photothermally triggered reaction involving deposition of thermal energy into adsorbate vibrations. (B-G) Adapted, with permission, from [6].

In several recently published review articles [17,39–41], a diverse range of plasmon-driven photocatalytic reactions discovered by SERS/TERS measurements have been summarized, alongside some insightful knowledge about the underlying reaction mechanisms extracted from steady-state and time-resolved spectroscopic results. Instead of providing a broad survey of all types of plasmon-driven photocatalytic reactions ever reported in the literature, this review focuses on a prototypical reaction system involving reductive coupling of nitroarene derivatives chemisorbed on nanostructured metal surfaces to showcase the latest advancements in development of experimental methodologies and data-analysis strategies. By going through a selection of case studies, this review will elaborate on how to pinpoint the exact roles of plasmonic hot carriers, distinguish thermal and nonthermal contributions, and elucidate the effects of metal–adsorbate interactions on molecular reactivity through rigorous analysis of the rich information provided by deliberately designed SERS/TERS measurements.

Plasmonic hot electron-driven reaction mechanisms

Although SERS and TERS are both considered as noninvasive tools for molecular fingerprinting in general, some plasmon-reactive adsorbate molecules may undergo interesting photocatalytic reactions during SERS/TERS measurements. One striking example is *para*-nitrothiophenol (pNTP) chemisorbed on metal surfaces, which dimerizes to produce *p,p′*-dimercaptoazobenzene (DMAB) with the aid of plasmons (Figure 2A) [42–46]. Time-resolved SERS results reported by Kim and coworkers [47] provide compelling experimental evidence for a hot electron-driven reaction mechanism. The samples for SERS measurements are composed of a self-assembled monolayer (SAM) of pNTP sandwiched between an Ag nanoparticle (AgNP) and an Au thin film (AuTF). When illuminated by a continuous-wave (cw) visible laser (633 nm), each AgNP/pNTP/AuTF junction serves as a dual-functional hot spot, providing hot electron flux for photocatalysis and local-field enhancements for SERS (Figure 2B). At the initial stage of the reaction, the characteristic nitro-stretching (ν_{NO2}, 1342 cm^{-1}) peak of pNTP is rapidly down-shifted by ~6 cm^{-1} before its intensity starts to decay (Figure 2C,D), signifying the formation of an anionic radical, *p*NTP•$^{-}$, upon injection of a single hot electron into a pNTP molecule [47–49]. Further reduction of *p*NTP•$^{-}$ may occur upon injection of additional hot electrons, and the overall buildup rate of DMAB is determined by the consumption rate of the anionic pNTP•$^{-}$ rather than the neutral pNTP. The pNTP•$^{-}$-to-DMAB conversion is signified by intensity decay of the ν_{NO2} peak of pNTP•$^{-}$ and

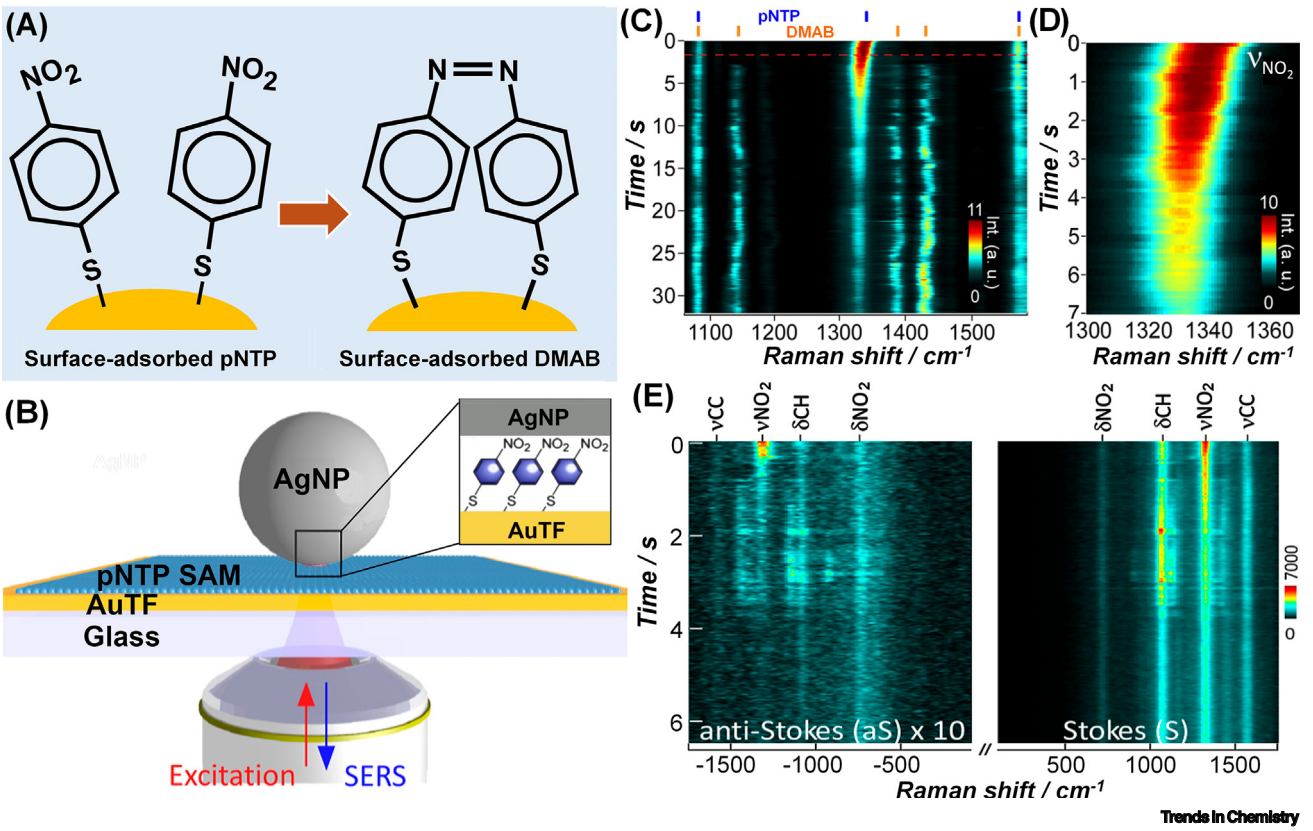

Figure 2. Hot electron injection and mode-selective vibrational excitation. (A) Schematic illustration of plasmon-driven reductive coupling of *para*-nitrothiophenol (pNTP) chemisorbed on a metal surface. (B) Schematic illustration of a pNTP self-assembled monolayer (SAM) sandwiched between an Ag nanoparticle (AgNP) and an Au thin film (AuTF). (C) Temporal evolution of surface-enhanced Raman scattering (SERS) spectra collected from an AgNP/pNTP/AuTF junction. (D) Zoomed-in view of panel (C) in the wavenumber range of 1300–1370 cm^{-1} within the first 7 s of reaction. (E) Time-resolved Stokes and anti-Stokes SERS spectra collected from an AgNP/pNTP/AuTF hotspot. Adapted, with permission, from (B–D) [47] and (E) [50]. Abbreviation: DMAB, *p,p′*-dimercaptoazobenzene.

emergence of the azo (ν_{NN}, 1389 and 1430 cm^{-1}) and CN stretching (ν_{CN}, 1143 cm^{-1}) peaks of DMAB in SERS spectra (Figure 2C). Although several other intermediates remain spectroscopically irresolvable, hot electron-induced formation of pNTP•$^{-}$ has been clearly identified as a critical elementary step at the early stage of the multistep pNTP coupling reactions.

The transient anionic radical produced upon hot electron injection may relax to a vibrationally excited state after ejecting an electron back to the metallic substrate (Figure 1F). Such plasmon-induced vibrational activation is particularly effective when the anionic state of the adsorbate has a significantly modified and shifted potential energy surface in comparison to that of its neutral counterpart. Kim and coworkers [50] have observed that the ν_{NO2} mode of pNTP in an AgNP/pNTP/AuTF junction can be selectively excited via transient hot electron transfer to the lowest unoccupied molecular orbital (LUMO) of pNTP, which is antibonding in nature. Upon initiation of the reactions, vibrationally excited pNTP exhibits a pronounced anti-Stokes ν_{NO2} SERS peak, which vanishes within ~1 s (Figure 2E). The anti-Stokes ν_{NO2} peak decays more rapidly than its Stokes counterpart (Figure 2E) consisting of overlapping spectral features of both pNTP and *p*NTP•$^{-}$, which suggests that the plasmons selectively excite pNTP but not the coexisting pNTP•$^{-}$. A significant fraction (~20%) of the vibrationally excited pNTP is in the overtone-excited states, as evidenced by notable asymmetric broadening of the anti-Stokes ν_{NO2} peak. Such overtone-excited reactants are typically even more reactive than those in the first-excited vibrational states.

SERS-based ultrafast spectroscopy provides a unique means of correlating photophysical dynamics to chemical reactivity of molecular adsorbates in plasmonic hot spots over the picosecond timescale, which is directly relevant to hot electron transfer processes. An ultrafast SERS approach developed by Frontiera and coworkers [51] uses a femtosecond pump pulse to excite the plasmons and a time-delayed picosecond pulse to probe the molecular vibrations of pNTP on aggregated AgNPs (Figure 3A). Transient spectral features exhibiting the characteristic line-shape of **Fano resonances** are consistently observed for all prominent pNTP and DMAB vibrational modes in ultrafast SERS difference spectra (Figure 3B), which persist for approximately 10 ps after plasmon excitation. Such Fano resonance line-shape originates essentially from the interference between narrow-band Stokes-shifted Raman emission of adsorbate molecules and broadband plasmon-induced photoluminescence of Ag, which arises from radiative recombination of hot electrons and holes. Fitting of the extracted amplitudes of the 1139 cm^{-1} mode yields a lifetime around 4 ps (Figure 3C), which matches the lifetimes of plasmonic hot electrons reported in the literature. pNTP molecules in strongly photoluminescent hot spots (high hot electron population in Ag) are observed to be significantly more reactive toward the coupling reactions than those residing in weakly photoluminescent hot spots (Figure 3D,E). These ultrafast SERS results strongly suggest that hot electrons are transferred from Ag to pNTP following Landau damping rather than being directly excited in a pNTP orbital through chemical interface damping.

With the aid of metallic nanocatalysts, nitrophenyl derivatives can also be chemically reduced through direct or transfer hydrogenation reactions with hydrogen gas or other hydrogen-storing species, such as borohydride and formate, serving as the hydrogen donors [52–54]. In contrast to the plasmon-driven reactions, catalytic (transfer)hydrogenation of nitroarenes under thermal conditions may lead to formation of aniline derivatives, while the aromatic azo compounds have been identified, in multiple cases, as critical intermediates in these multistep reduction reactions [55–57]. Interestingly, plasmonic hot electrons in metallic nanocatalysts can also be harnessed to kinetically modulate the chemical reduction of nitrophenyl derivatives [58]. Results of density functional theory (DFT) calculations further suggest that population of electrons in the LUMO of nitrophenol elongates the N–O bond, which effectively triggers the N–O bond cleavage and the subsequent stepwise hydrogenation processes [59].

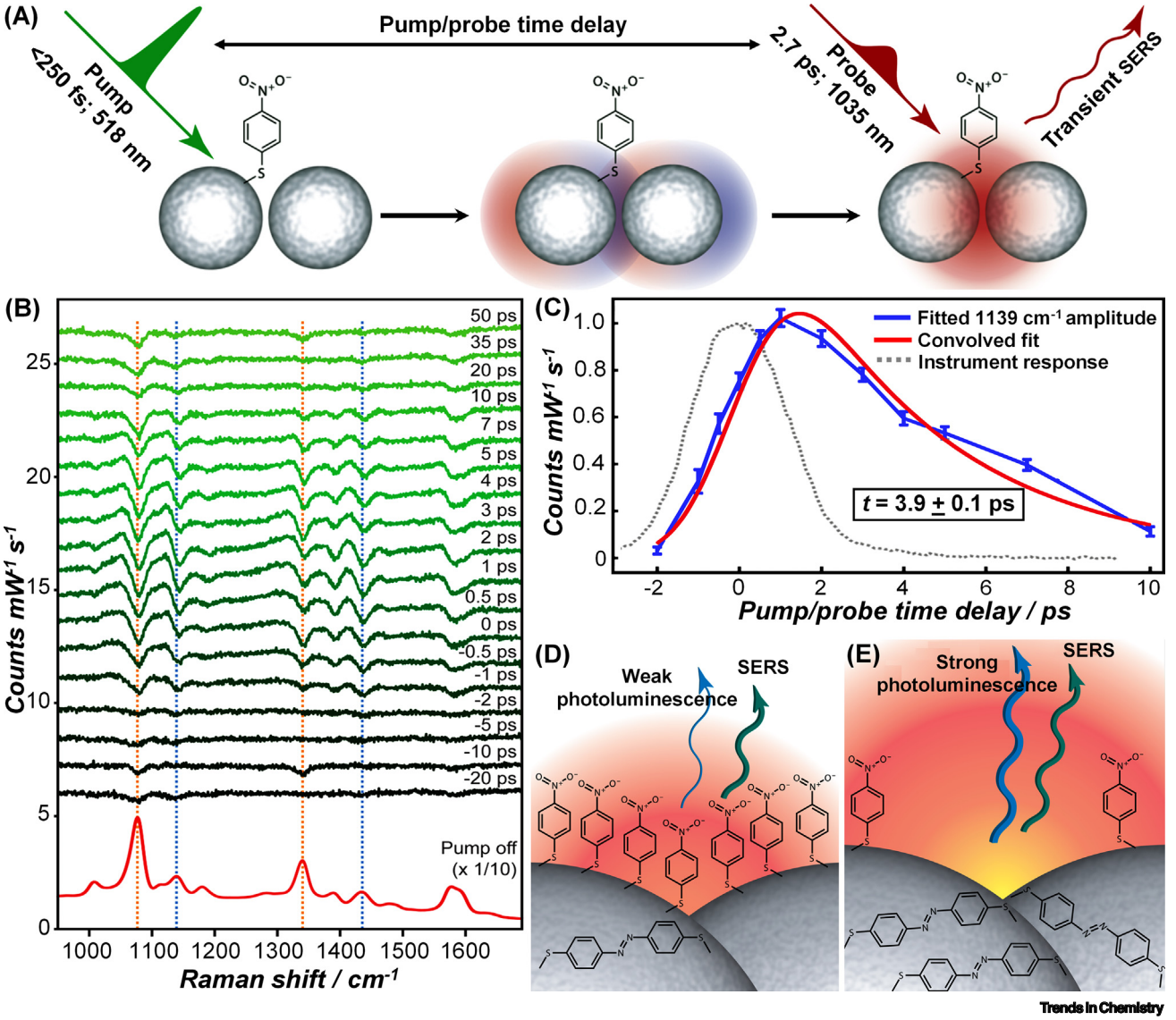

Figure 3. Correlation between hot electron population and molecular reactivity. (A) Schematic representation of ultrafast pump/probe surface-enhanced Raman scattering (SERS) measurements. (B) Ultrafast SERS difference spectra (processed by subtracting SERS spectra taken with the pump pulse blocked from identical spectra collected with the pump pulse present) taken at time delays ranging from –20 to +50 ps. (C) Fitted amplitude of the transient feature at 1139 cm^{-1} shown in (B). Schematic representation of (D) low reactivity and (E) high reactivity hot spots. Adapted, with permission, from [51].

To meet the energetic requirement for Ag-to-pNTP transfer of hot electrons, the wavelengths of excitation photons must be shorter than ~700 nm because the LUMO energy of pNTP chemisorbed to Ag is ~1.7 eV above the Ag Fermi energy [60]. Interestingly, the plasmon-driven pNTP reduction can still occur on nanostructured Ag surfaces through alternative electron transfer pathways even at excitation wavelengths longer than 700 nm. Employing SERS as an *in situ* spectroscopic tool, Wang and coworkers [61] have studied the reductive coupling of pNTP on individual Fe_3O_4@Ag photocatalyst particles under near-infrared cw excitations (785 nm) in an atmosphere-controlled environment. Each photocatalyst particle is composed of a magnetite (Fe_3O_4) core densely decorated with Ag nanocubes, a suprananostructure possessing broadband

near-infrared plasmon resonances and highly abundant hot spots in the junctions between adjacent nanocubes. Under near-infrared illumination, the pNTP coupling reactions proceed rapidly in an O_2 atmosphere or in ambient air but get completely suppressed in an anaerobic N_2 atmosphere. Benefiting from the close energetic alignment between the antibonding $2\pi^*$ orbital of O_2 and the Fermi level of Ag, near-infrared light-excited hot electrons in Ag can be transferred to surface-adsorbed O_2, instead of the pNTP adsorbates, to generate transient $O_2^{\bullet-}$ radicals [61–63], which serve as a carrier-relaying species activating the pNTP adsorbates for the coupling reactions [61].

Distinguishing thermal and nonthermal effects

Both nonthermal plasmonic effects and photothermal heating can contribute to the kinetic enhancement of a plasmon-driven reaction. However, it remains an immensely challenging task to unambiguously delineate the nonthermal and thermal contributions [22,64–69]. A widely utilized experimental strategy involves careful examination of the dependence of reaction rate on excitation light intensity [70,71]. As exemplified by multiple case studies, the reaction rates appear linearly proportional to the excitation power (P_{ex}) under moderate cw illumination but may switch to a superlinear P_{ex}-dependence when P_{ex} exceeds certain threshold values or under femtosecond-pulsed laser illumination, an interesting phenomenon that may originate from multiple effects, such as photothermal heating at metal–adsorbate interfaces (Arrhenius-type temperature dependence) [72], multiphoton absorption stimulated by high photon flux density [4,9], and plasmonic modulation of activation energy (E_a) [65,73]. To further quantify the thermal and nonthermal contributions, the local temperatures at adsorbate-occupying active sites on metallic photocatalyst surfaces must be precisely measured, ideally under operando conditions. The light-induced thermal gradients over the photocatalyst surfaces, nonequilibrated thermal energy partition, and intrinsic complexity and uncertainty associated with such nanothermometric measurements have led to inconsistent or even contradictory conclusions drawn from previous studies, not only in the case of reductive pNTP coupling reactions [74–77], but also for a series of other plasmon-driven photocatalytic reactions [65,78,79]. Plasmon-enhanced Raman spectroscopy provides unique nanothermometric tools for probing the electronic temperatures in light-illuminated metallic nanostructures and the vibrational temperatures in molecular adsorbates [28,74,77,80–83], which may help clarify some widely debated controversies in the literature. With recent advancements in high-resolution SERS/TERS-based nanothermometry, it has become possible to precisely measure the local temperatures in single plasmonic hot spots [84] and even the effective temperature of a single molecule in a hot spot [85].

Photon scattering from metallic nanostructures bearing Fermi–Dirac distribution of hot electrons gives rise to a broad background in anti-Stokes SERS spectra, which provide information about the local temperatures in metallic nanostructures (Box 1) [28,77,81,82]. For the pNTP coupling reactions on aggregated Au nanoflowers under near-infrared cw laser illumination, the reaction rates have been observed to exhibit Arrhenius-like behaviors with respect to both the local temperature in nanoparticles (quantified by the anti-Stokes nanothermometry) and the externally controlled reaction temperature [77]. Although the reactions cannot be activated solely by external heating, the overall reaction kinetics are determined predominantly by photothermal heating rather nonthermal plasmonic effects, strongly suggesting that plasmons can selectively lower the E_a of the initial photoactivation step, which most likely involves the injection of hot electrons into molecular adsorbates, whereas the rate-limiting step (i.e., the bimolecular coupling of activated pNTP) remains thermally controlled.

The local temperature the molecular adsorbates experience, however, may differ substantially from the electronic temperature in metallic nanostructures. In a normal Raman spectrum, the ratio between anti-Stokes and Stokes peak intensities of a vibrational mode can be utilized to

Box 1. Nanothermometry based on anti-Stokes background intensities

The local temperature in a light-illuminated plasmonic nanoparticle can be measured based on the intensity of the background signals in anti-Stokes SERS spectra [28,77,81,82]. The anti-Stokes background intensity is related to the rate of anti-Stokes emission in response to the relaxation of hot electrons whose energy distribution profile follows the Fermi–Dirac distribution. The equilibrated temperature in nanoparticles can be extracted by fitting the anti-Stokes background with the follow equation:

$$I_{\mathrm{aS,background}} = \frac{I_{\mathrm{aS,0}}}{\exp\left(\frac{E_{\mathrm{Raman}}}{k_{\mathrm{B}}T}\right) + 1} \quad [\mathrm{I}]$$

where $I_{\mathrm{aS,background}}$ is the anti-Stokes background intensity at a Raman shift energy (E_{Raman}), $I_{\mathrm{aS,0}}$ is the anti-Stokes background intensity at E_{Raman} of 0, k_{B} is the Boltzmann constant, and T is temperature.

However, as pointed out by Baffou in a perspective article [82], some controversies exist in the literature regarding the origin of the anti-Stoke background in SERS spectra and the appropriate statistical models that should be used for the anti-Stokes nanothermometry. The inelastic light emission from metallic nanoparticles may originate from electronic Raman scattering or photoluminescence. It remains challenging to clearly distinguish the two mechanisms and the involvement of one or the other may depend on the structure and morphology of the nanoparticles as well as detailed measurement conditions. To describe the electron occupation $f(E,T)$ near the Fermi level, Fermi–Dirac distribution is the natural occupation statistics widely adopted by the solid-state physics community for decades:

$$f_{\mathrm{Fermi-Dirac}}(E,T) = \frac{1}{\exp\left(\frac{E}{k_{\mathrm{B}}T}\right) + 1} \quad [\mathrm{II}]$$

where E is the energy of the electrons relative to the Fermi energy. However, it was recently argued that the electrons near the Fermi level follow Bose-Einstein statistics instead because of the electron–phonon interactions:

$$f_{\mathrm{Bose-Einstein}}(E,T) = \frac{1}{\exp\left(\frac{E}{k_{\mathrm{B}}T}\right) - 1} \quad [\mathrm{III}]$$

Such subtlety was further discussed by Orrit and coworkers [99], who noticed that the difference between the two statistic models is rather insignificant within the experimentally measured spectral range of anti-Stokes shifts, except in the small energy shift range below ~600 cm^{-1}. Therefore, both Fermi–Dirac and Bose–Einstein distributions can be utilized for curve fitting in many cases and can even be substituted with the Boltzmann statistics for further convenience:

$$f_{\mathrm{Boltzmann}}(E,T) = \exp\left(-\frac{E}{k_{\mathrm{B}}T}\right) \quad [\mathrm{IV}]$$

calculate the temperature of molecular vibrations based on the Boltzmann distribution (Box 2). However, in SERS/TERS spectra, the anti-Stokes-to-Stokes intensity ratios not only depend on temperature but are also profoundly influenced by other factors, such as the non-equivalent local-field enhancements at anti-Stokes and Stokes emission frequencies [74,83] and vibrational pumping caused by electron injection into the adsorbates [28,29], which introduces substantial complications and uncertainty to nanothermometric measurements. Choosing molecular probes with intrinsically temperature-dependent SERS features provides a more straightforward and reliable nanothermometry approach based solely on the Stokes Raman shifts without the need to analyze the anti-Stokes signals [86–88]. Chen and Wang [89] have developed a nanothermometry using thiophenol chemisorbed to Ag as a temperature-sensitive SERS probe. AgNPs are assembled into hexagonally close-packed arrays, which serve as SERS substrates, photothermal transducers, and plasmonic photocatalysts simultaneously (Figure 4A,B). The intensity ratio between the β_{CC} (1000 cm^{-1}) and ν_{CS} (1072 cm^{-1}) modes in the SERS spectra of thiophenol exhibits a linear dependence on externally controlled temperature within the range of 20–120°C (Figure 4C,D), which enables real-time monitoring of local temperature evolution in hot spots under light illumination. The photothermal heating appears significantly more efficient in

Box 2. Raman thermometry based on anti-Stokes-to-Stokes peak intensity ratios

For a particular vibrational mode, the ratio of intensities at its anti-Stokes and Stokes frequencies in the normal Raman spectrum can be used to calculate the vibrational temperature of the molecules based on a Boltzmann distribution of the ground and first excited state populations. The temperature-dependence of anti-Stokes-to-Stokes intensity ratio can be expressed by the following equation:

$$\frac{I_{aS}}{I_S} = \frac{(\nu_l + \nu_v)^4}{(\nu_l - \nu_v)^4} \exp\left(-\frac{h\nu_v}{k_B T}\right) \quad [I]$$

where I_{aS} is the intensity of the anti-Stokes Raman peak, I_S is the intensity of the Stokes Raman peak, ν_l is the frequency of the excitation laser, ν_v is the vibrational frequency of the Raman mode, h is Planck constant, k_B is Boltzmann constant, and T is the temperature.

When extending this thermometric approach from normal Raman to SERS and TERS, the situation becomes substantially more complicated. In SERS/TERS, the anti-Stokes-to-Stokes intensity ratios are determined not only by the temperature but also by the nonequivalent local-field enhancements at anti-Stokes and Stokes emission frequencies and vibrational pumping caused by electron injection into the adsorbates. In some nanoparticle/adsorbate systems, even ostensible plasmon-induced molecular cooling has been recently observed according to the anti-Stokes-to-Stokes scattering intensity ratios in SERS spectra [100], strongly suggesting that such nanothermometric measurements of local vibrational temperatures in molecular adsorbates may be further complicated by some unrecognized plasmon–molecule interactions.

air than in water (Figure 4E), a direct consequence of different heat dissipation rates caused by the difference in thermal conductivities of the reaction media (~0.60 W m^{-1} K^{-1} for water and 0.025 W m^{-1} K^{-1} for air). Changing the reaction medium from air to water significantly modifies not only the apparent rate of the plasmon-driven pNTP coupling reactions, but also the P_{ex}-dependence profile of the rate constant, k_{obs} (Figure 4F). When fitting the experimentally measured P_{ex}-dependence of k_{obs}, both nonthermal (linear P_{ex}-dependence) and thermal (Arrhenius relationship) contributions should be taken into consideration (see the equation in the inset of Figure 4F, where B is a fractional coefficient, E_a is the activation energy associated with the rate-limiting step, R is the molar gas constant, T_0 is the ambient temperature in dark in the unit of K, and c is a photothermal transduction coefficient carrying the unit of K mW^{-1}). The values of E_a extracted from curve fitting appear essentially independent of the thermal conductivity of the reaction medium (Figure 4F). These results shed light on the crucial roles that photothermal heating may play in kinetic modulation of the rate-limiting steps in plasmon-driven photocatalytic reactions.

Effects of metal-adsorbate interactions on molecular reactivities

Although driven by plasmonic hot electrons, the reductive pNTP coupling reactions are kinetically limited by the dimerization step. TERS studies conducted by Ren and coworkers [90] reveal that the bimolecular coupling between nitro groups is facilitated when pNTP adsorbates are oriented at specific tilt angles with respect to Ag(111) and Au(111) surfaces. The structural flexibility of surface-adsorbed pNTP directly determines the molecular reactivity because the dimerization process involves rearrangements of adsorbate conformations on the metal surfaces. Combing TERS imaging with scanning tunneling microscopy and DFT calculations, Zenobi, Kumar, and coworkers [91] have investigated detailed structure–reactivity relationships for plasmon-driven pNTP coupling reactions on a single-crystalline Au(111) surface and a polycrystalline, template-stripped Au (TS-Au) substrate (Figure 5A). Kinetically driven disordered phase and thermodynamically stable ordered phase of pNTP SAMs are constructed via drop-cast and immersion protocols, respectively. A significantly higher catalytic efficiency is observed in the disordered phase than in the ordered phase (Figure 5B). Interestingly, pNTP SAMs on locally curved TS-Au surfaces are structurally less ordered than those on Au(111) surfaces, thereby exhibiting higher reactivity toward the reductive coupling reactions. An interesting analog of pNTP is *para*-nitrobenzyl mercaptan (pNBM), in which an additional methylene group is inserted between the thiol and the

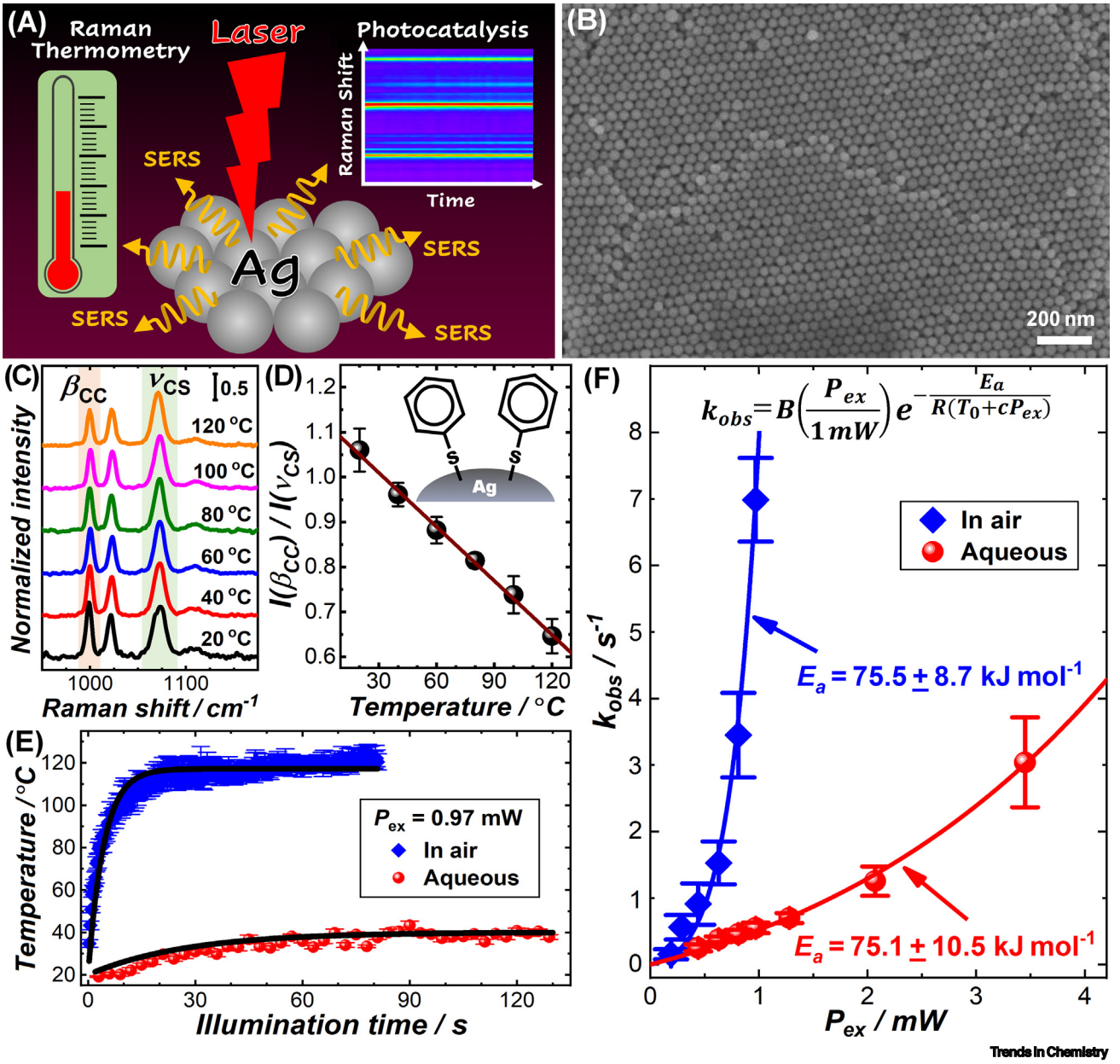

Figure 4. Nonthermal and thermal effects on plasmonic photocatalysis. (A) Schematic illustration of using close-packed Ag nanoparticle arrays as triple-functional substrates for plasmonic photocatalysis, photothermal transduction, and surface-enhanced Raman scattering (SERS) measurements. (B) Scanning electron microscope image of Ag nanoparticle arrays assembled on an Si substrate. (C) Representative SERS spectra of thiophenol on Ag nanoparticle arrays at various temperatures. The intensities of the ν_{CS} mode (1076 cm^{-1}) were normalized to 1 for comparison. (D) Temperature-dependence of the peak intensity ratios between the β_{CC} mode and the ν_{CS} mode. (E) Temporal evolution of the local temperatures in the hot spots under continuous laser illumination (785 nm, 0.97 mW, and ~2 μm focal spot diameter) in an aqueous medium and in air. (F) Excitation power (P_{ex})-dependence of k_{obs} for plasmon-driven *para*-nitrothiophenol (pNTP) coupling reactions in air and in an aqueous environment. Adapted, with permission, from [89].

nitrophenyl groups. Similar to pNTP, pNBM can also undergo plasmon-driven reductive coupling reactions to produce 4,4′-dimercaptomethanazobenzene (DMMA). As reported by Bargheer and coworkers [92], pNBM chemisorbed on Au surfaces dimerizes more rapidly and efficiently than its pNTP counterpart under identical light illumination conditions, because the methylene group

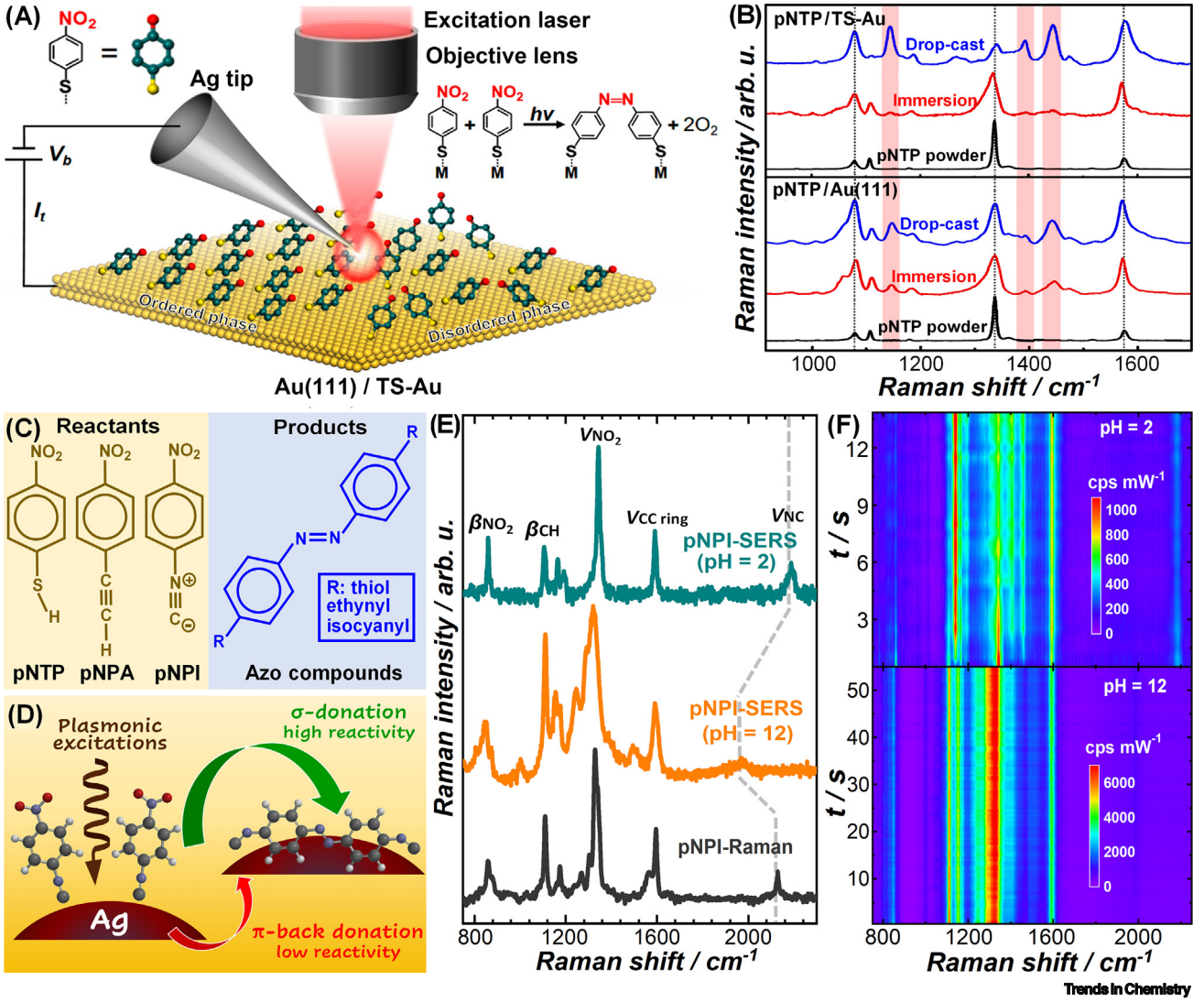

Figure 5. Effects of metal–adsorbate interactions on molecular reactivity. (A) Schematic diagram of the tip-enhanced Raman scattering (TERS) setup used for investigating reactive arrangement in photocatalytic coupling of *para*-nitrothiophenol (pNTP) on template-stripped polycrystalline Au substrates (TS-Au) and single-crystalline Au(111) surfaces. (B) TERS spectra of pNTP-functionalized (upper panel) TS-Au and (lower panel) Au(111) surfaces prepared via drop-cast (blue trace) or immersion (red trace) protocols. The Raman spectrum of pNTP powder (black trace) is also plotted for comparison. Characteristic p,p′-dimercaptoazobenzene (DMAB) peaks at 1146, 1390, and 1442 cm^{-1} are highlighted in red. (C) Chemical structures of pNTP, para-nitrophenylacetylene (pNPA), para-nitrophenylisocyanide (pNPI), and the aromatic azo compounds produced through the plasmon-driven reductive coupling reactions. (D) Scheme illustrating how the chemical nature of the metal–adsorbate interactions modulates the plasmonic reactivity of nitrophenyl derivatives. (E) Experimentally measured normal Raman spectrum of pNPI and SERS spectra of pNPI chemisorbed to Ag nanoparticle surfaces at pHs of 2 and 12. (F) Time-resolved SERS spectra collected from pNPI chemisorbed to Ag nanoparticle surfaces at pHs of (upper panel) 2 and (lower panel) 12 under continuous illumination by a 785 nm laser at an excitation power (P_{ex}) of 2.64 mW. Adapted, with permission, from (A,B) [91] and (C–F) [98].

endows pNBM with additional degrees of freedom for orientational rearrangements on Au surfaces. All these observations clearly reveal that the rate-limiting dimerization step in plasmon-driven nitroarene coupling reactions can be kinetically boosted by enhancing the structural flexibility of adsorbates.

The orientational arrangements and structural flexibility of molecular adsorbates are intimately tied to the chemical nature of metal–adsorbate interactions. While thiolated molecules represent so

far, the most intensively studied adsorbate system on metal surfaces [93], other nonthiolated surface-anchoring groups, such as terminal alkyne [94], diazonium [95], N-heterocyclic carbene [96], and isocyano groups [97], can also be utilized by organic molecules to form covalent interactions with metallic substrates. Through SERS measurements, Chen and Wang [98] have characterized the bonding nature of metal–adsorbate interactions in three representative nitrophenyl derivatives, specifically pNTP, *para*-nitrophenylacetylene (pNPA), and *para*-nitrophenylisocyanide (pNPI), and further compared their plasmonic reactivities toward the reductive coupling reactions (Figure 5C). A chemisorbed pNTP molecule uses its thiol group to interact with AgNPs through **σ-donation**, whereas the interactions between the ethynyl group in pNPA and AgNP surfaces are dominated by strong **π-back donation**, which is evidenced by a significant spectral downshift of the C≡C vibrational mode in SERS spectra. pNPA remains significantly less reactive than pNTP under a broad range of reaction conditions, suggesting that switching the adsorbate-binding mode from σ-donation to π-back donation leads to decreased molecular reactivity (see schematic illustration in Figure 5D). The chemical nature of the interactions between the isocyano group in pNPI and metallic Ag is found to be even more complicated and versatile than Ag-thiol and Ag-ethynyl interactions, exhibiting π-back donation characteristics in an alkaline environment (downshift of N≡C stretching mode) but switching to the σ-donation mode (upshift of N≡C stretching mode) in an acidic environment (Figure 5E). Consequently, pNPI chemisorbed on AgNP surfaces becomes more reactive when decreasing the pH of reaction medium (Figure 5F). Switching the chemisorption mode from π-back donation to σ-donation not only optimizes the surface orientations but also increases the structural flexibility of nitrophenyl derivative adsorbates, which effectively accelerates the biomolecular coupling processes.

Concluding remarks

While the library of plasmon-driven photocatalytic reactions has continued to expand over the past decade, many critical aspects concerning the detailed mechanisms involved in plasmonic photocatalysis remain elusive due to the intricate interplay among multiple plasmonic photophysical and photochemical effects over a broad range of timescales. Combining ultrahigh surface-sensitivity with molecular fingerprinting and time-resolving capabilities, plasmon-enhanced Raman spectroscopy provides a vibrational spectroscopic tool, particularly useful for detailed mechanistic studies of plasmonic photocatalysis. Through time-resolved SERS/TERS measurements, dynamic transforming behaviors of molecular adsorbates can be fine-resolved in real time, enabling unambiguous identification of critical transient intermediates and the underlying hot carrier transfer channels. In addition, integration of kinetic and nanothermometric measurements using SERS/TERS provides a unique way to correlate detailed kinetic characteristics to local temperatures at the active sites in hot spots, which paves the avenue toward quantitative understanding of thermal and nonthermal effects. Furthermore, using SERS/TERS as *in situ* molecular fingerprinting tools, the plasmonic reactivity of molecular adsorbates can be directly correlated to the exact chemical nature of metal–adsorbate interactions. Although this review focuses on a prototypical model reaction system, the experimental methodologies and data analysis strategies can be broadly applied to mechanistic studies of other plasmon-driven reactions as well. The insights gained from deliberately designed SERS/TERS measurements form a crucial knowledge framework guiding the rational design of catalyst–adsorbate systems with optimized light-matter and plasmon–molecule interactions, based upon which improved light-harvesting efficiency, precise kinetic modulation, and targeted chemoselectivity can be achieved through plasmonic photocatalysis. An intrinsic limitation of SERS and TERS is that they are only capable of probing the transforming behaviors of molecules residing in localized hot spots, which account for a small fraction of the molecular adsorbates over the entire catalyst surface, because the spectroscopic signals are dominated by molecules experiencing the highest local field enhancements. It also remains challenging to resolve the signals of transient intermediates exhibiting short

Outstanding questions

How can we capture and identify short-lived transient species in a multistep plasmon-driven photocatalytic reaction through *in situ* SERS/TERS measurements with desired time resolutions?

How can we develop ultrafast SERS/TERS approaches capable of probing molecular responses at the early stages of plasmon decay over timescales ranging from femtoseconds to picoseconds?

How can we develop generic SERS/TERS-based nanothermometry for precise and reliable measurements of local temperatures in hot spots that are broadly applicable to a diverse range of metal–adsorbate systems?

How can we image the spatial distribution of photocatalytically active sites in hot spots with nanoscale precision using super-resolution SERS/TERS imaging approaches?

How can we resolve and analyze plasmon-mediated dynamic transforming behaviors of single molecules or a few molecules in a single hot spot through SERS/TERS measurements?

How can we utilize SERS/TERS to study plasmon-driven photocatalytic reactions on the surfaces of nonmetal plasmonic materials, such as degenerately doped semiconductor nanostructures?

lifetimes, intrinsically low Raman cross-sections, and spectroscopic features that overlap with those of the reactants and products. Further advancement in fundamental understanding of plasmonic photocatalysis relies critically on development of new SERS/TERS spectroscopy/imaging tools with desired temporal and spatial resolutions, streamlined high-throughput data analysis, and deliberate control over both materials structures and local chemical environments in plasmonic hot spots (see Outstanding questions).

Acknowledgments

This work is supported by the Macromolecular, Supramolecular, and Nanochemistry Program in the Division of Chemistry of the National Science Foundation (NSF) of the USA under Grant CHE-2202928. The content is solely the responsibility of the author and does not necessarily represent the official views of the NSF.

Declaration of interests

The author declares no competing interests.

References

1. Brongersma, M.L. *et al.* (2015) Plasmon-induced hot carrier science and technology. *Nat. Nanotechnol.* 10, 25–34
2. Govorov, A.O. *et al.* (2014) Photogeneration of hot plasmonic electrons with metal nanocrystals: quantum description and potential applications. *Nano Today* 9, 85–101
3. Gellé, A. *et al.* (2020) Applications of plasmon-enhanced nanocatalysis to organic transformations. *Chem. Rev.* 120, 986–1041
4. Kale, M.J. *et al.* (2014) Direct photocatalysis by plasmonic nanostructures. *ACS Catal.* 4, 116–128
5. Kherbouche, I. *et al.* (2020) Plasmon-mediated surface functionalization: new horizons for the control of surface chemistry on the nanoscale. *Chem. Mater.* 32, 5442–5454
6. Kazuma, E. and Kim, Y. (2019) Mechanistic studies of plasmon chemistry on metal catalysts. *Angew. Chem. Int. Ed.* 58, 4800–4808
7. Jain, V. *et al.* (2022) Plasmonic photocatalysis: activating chemical bonds through light and plasmon. *Adv. Opt. Mater.* 10, 2200463
8. Zhang, Y.C. *et al.* (2018) Surface-plasmon-driven hot electron photochemistry. *Chem. Rev.* 118, 2927–2954
9. Christopher, P. *et al.* (2012) Singular characteristics and unique chemical bond activation mechanisms of photocatalytic reactions on plasmonic nanostructures. *Nat. Mater.* 11, 1044–1050
10. Fang, M. *et al.* (2021) Recent progress on metal-enhanced photocatalysis: a review on the mechanism. *Research* 2021, 9794329
11. Besteiro, L.V. *et al.* (2019) The fast and the furious: ultrafast hot electrons in plasmonic metastructures. Size and structure matter. *Nano Today* 27, 120–145
12. Christopher, P. and Moskovits, M. (2017) Hot charge carrier transmission from plasmonic nanostructures. *Annu. Rev. Phys. Chem.* 68, 379–398
13. Cortés, E. (2017) Efficiency and bond selectivity in plasmon-induced photochemistry. *Adv. Opt. Mater.* 5, 1700191
14. Sytwu, K. *et al.* (2019) Bimetallic nanostructures: combining plasmonic and catalytic metals for photocatalysis. *Adv. Phys. X* 4, 1619480
15. Jiang, W. *et al.* (2023) Active site engineering on plasmonic nanostructures for efficient photocatalysis. *ACS Nano* 17, 4193–4229
16. Carlin, C.C. *et al.* (2023) Nanoscale and ultrafast in situ techniques to probe plasmon photocatalysis. *Chem. Phys. Rev.* 4, 041309
17. Warkentin, C.L. *et al.* (2021) Decoding chemical and physical processes driving plasmonic photocatalysis using surface-enhanced Raman spectroscopies. *Acc. Chem. Res.* 54, 2457–2466
18. Cortés, E. *et al.* (2022) Experimental characterization techniques for plasmon-assisted chemistry. *Nat. Rev. Chem.* 6, 259–274
19. Yang, J.H. *et al.* (2018) Emerging applications of plasmons in driving CO_2 reduction and N_2 fixation. *Adv. Mater.* 30, 1802227
20. Yuan, L. *et al.* (2023) Sustainable chemistry with plasmonic photocatalysts. *Nanophotonics* 12, 2745–2762
21. Fusco, Z. and Beck, F.J. (2024) Advances in fundamentals and application of plasmon-assisted CO_2 photoreduction. *Nanophotonics* 13, 387–417
22. Cortés, E. *et al.* (2020) Challenges in plasmonic catalysis. *ACS Nano* 14, 16202–16219
23. Zhan, C. *et al.* (2020) Recent progress and prospects in plasmon-mediated chemical reaction. *Matter* 3, 42–56
24. Kazuma, E. (2024) Key factors for controlling plasmon-induced chemical reactions on metal surfaces. *J. Phys. Chem. Lett.* 15, 59–67
25. Kazuma, E. *et al.* (2018) Real-space and real-time observation of a plasmon-induced chemical reaction of a single molecule. *Science* 360, 521–525
26. Tesema, T.E. *et al.* (2020) Extracting electronic transition bands of adsorbates from molecule-plasmon excitation coupling. *J. Phys. Chem. Lett.* 11, 3507–3514
27. Mukherjee, S. *et al.* (2013) Hot electrons do the impossible: plasmon-induced dissociation of H_2 on Au. *Nano Lett.* 13, 240–247
28. Boerigter, C. *et al.* (2016) Mechanism of charge transfer from plasmonic nanostructures to chemically attached materials. *ACS Nano* 10, 6108–6115
29. Boerigter, C. *et al.* (2016) Evidence and implications of direct charge excitation as the dominant mechanism in plasmon-mediated photocatalysis. *Nat. Commun.* 7, 10545
30. Langer, J. *et al.* (2020) Present and future of surface-enhanced Raman scattering. *ACS Nano* 14, 28–117
31. Wang, X. *et al.* (2020) Fundamental understanding and applications of plasmon-enhanced Raman spectroscopy. *Nat. Rev. Phys.* 2, 253–271
32. Ding, S.Y. *et al.* (2017) Electromagnetic theories of surface-enhanced Raman spectroscopy. *Chem. Soc. Rev.* 46, 4042–4076
33. Sharma, B. *et al.* (2012) SERS: materials, applications, and the future. *Mater. Today* 15, 16–25
34. Halas, N.J. *et al.* (2011) Plasmons in strongly coupled metallic nanostructures. *Chem. Rev.* 111, 3913–3961
35. Zhang, Q.F. *et al.* (2014) Gold nanoparticles with tipped surface structures as substrates for single-particle surface-enhanced Raman spectroscopy: concave nanocubes, nanotrisoctahedra, and nanostars. *ACS Appl. Mater. Interfaces* 6, 17255–17267
36. Xie, J.P. *et al.* (2008) The synthesis of SERS-active gold nanoflower tags for *in vivo* applications. *ACS Nano* 2, 2473–2480
37. Zhang, Q.F. *et al.* (2014) Porous Au nanoparticles with tunable plasmon resonances and intense field enhancements for single-particle SERS. *J. Phys. Chem. Lett.* 5, 370–374

38. Bailo, E. and Deckert, V. (2008) Tip-enhanced Raman scattering. *Chem. Soc. Rev.* 37, 921–930
39. Chen, K.X. and Wang, H. (2021) Plasmon-driven photocatalytic molecular transformations on metallic nanostructure surfaces: mechanistic insights gained from plasmon-enhanced Raman spectroscopy. *Mol. Syst. Des. Eng.* 6, 250–280
40. Zhan, C. *et al.* (2019) Plasmon-mediated chemical reactions on nanostructures unveiled by surface-enhanced Raman spectroscopy. *Acc. Chem. Res.* 52, 2784–2792
41. Li, Z.D. and Kurouski, D. (2021) Plasmon-driven chemistry on mono- and bimetallic nanostructures. *Acc. Chem. Res.* 54, 2477–2487
42. Chen, X.J. *et al.* (2014) Surface-enhanced Raman spectroscopy toward application in plasmonic photocatalysis on metal nanostructures. *J Photochem Photobiol C: Photochem Rev* 21, 54–80
43. Sun, M.T. and Xu, H.X. (2012) A novel application of plasmonics: plasmon-driven surface-catalyzed reactions. *Small* 8, 2777–2786
44. Dong, B. *et al.* (2011) Substrate-, wavelength-, and time-dependent plasmon-assisted surface catalysis reaction of 4-nitrobenzenethiol dimerizing to p,p'-dimercaptoazobenzene on Au, Ag, and Cu films. *Langmuir* 27, 10677–10682
45. Kang, L.L. *et al.* (2013) Laser wavelength- and power-dependent plasmon-driven chemical reactions monitored using single particle surface enhanced Raman spectroscopy. *Chem. Commun.* 49, 3389–3391
46. van Schrojenstein Lantman, E.M. *et al.* (2012) Catalytic processes monitored at the nanoscale with tip-enhanced Raman spectroscopy. *Nat. Nanotechnol.* 7, 583–586
47. Choi, H.K. *et al.* (2016) Identification of the first elementary step in the photocatalytic reduction of nitrobenzenethiols on a metallic surface. *J. Phys. Chem. Lett.* 7, 4099–4104
48. Wang, R. *et al.* (2020) Direct experimental evidence of hot carrier-driven chemical processes in tip-enhanced Raman spectroscopy (TERS). *J. Phys. Chem. C* 124, 2238–2244
49. Wang, C.F. *et al.* (2020) The prevalence of anions at plasmonic nanojunctions: a closer look at p-nitrothiophenol. *J. Phys. Chem. Lett.* 11, 3809–3814
50. Shin, H.H. *et al.* (2023) Vibrationally hot reactants in a plasmon-assisted chemical reaction. *J. Am. Chem. Soc.* 145, 12264–12274
51. Brandt, N.C. *et al.* (2016) Ultrafast surface-enhanced Raman probing of the role of hot electrons in plasmon-driven chemistry. *J. Phys. Chem. Lett.* 7, 3179–3185
52. Wunder, S. *et al.* (2010) Kinetic analysis of catalytic reduction of 4-nitrophenol by metallic nanoparticles immobilized in spherical polyelectrolyte brushes. *J. Phys. Chem. C* 114, 8814–8820
53. Corma, A. and Serna, P. (2006) Chemoselective hydrogenation of nitro compounds with supported gold catalysts. *Science* 313, 332–334
54. Wang, Z.X. *et al.* (2022) Colloidal polydopamine beads: a photothermally active support for noble metal nanocatalysts. *ACS Appl. Mater. Interfaces* 14, 17560–17569
55. Xie, W. *et al.* (2011) Synthesis of bifunctional Au/Pt/Au core/shell nanoraspberries for in situ SERS monitoring of platinum-catalyzed reactions. *J. Am. Chem. Soc.* 133, 19302–19305
56. Zhang, Q.F. *et al.* (2016) Facet Control of Gold Nanorods. *ACS Nano* 10, 2960–2974
57. Zhang, J.W. *et al.* (2016) Ag@Au concave cuboctahedra: a unique probe for monitoring Au-catalyzed reduction and oxidation reactions by surface-enhanced Raman spectroscopy. *ACS Nano* 10, 2607–2616
58. Barbosa, E.C.M. *et al.* (2018) Reaction pathway dependence in plasmonic catalysis: hydrogenation as a model molecular transformation. *Chem. Eur. J.* 24, 12330–12339
59. Mou, T. *et al.* (2021) Localized orbital excitation drives bond formation in plasmonic catalysis. *ACS Appl. Mater. Interfaces* 13, 60115–60124
60. Zhao, L.B. *et al.* (2014) Theoretical study of plasmon-enhanced surface catalytic coupling reactions of aromatic amines and nitro compounds. *J. Phys. Chem. Lett.* 5, 1259–1266
61. Zhang, Q.F. *et al.* (2019) Photothermal effect, local field dependence, and charge carrier relaying species in plasmon-driven photocatalysis: a case study of aerobic nitrothiophenol coupling reaction. *J. Phys. Chem. C* 123, 26695–26704
62. Zhang, Q. and Wang, H. (2018) Mechanistic insights on plasmon-driven photocatalytic oxidative coupling of thiophenol derivatives: evidence for steady-state photoactivated oxygen. *J. Phys. Chem. C* 122, 5686–5697
63. Huang, Y.F. *et al.* (2014) Activation of oxygen on gold and silver nanoparticles assisted by surface plasmon resonances. *Angew. Chem. Int. Ed.* 53, 2353–2357
64. Zhang, X. *et al.* (2018) Plasmon-enhanced catalysis: distinguishing thermal and nonthermal effects. *Nano Lett.* 18, 1714–1723
65. Zhou, L.A. *et al.* (2018) Quantifying hot carrier and thermal contributions in plasmonic photocatalysis. *Science* 362, 69–72
66. Kamarudheen, R. *et al.* (2018) Quantifying photothermal and hot charge carrier effects in plasmon-driven nanoparticle syntheses. *ACS Nano* 12, 8447–8455
67. Li, X. *et al.* (2019) Light-induced thermal gradients in ruthenium catalysts significantly enhance ammonia production. *Nano Lett.* 19, 1706–1711
68. Negrín-Montecelo, Y. *et al.* (2022) Plasmonic photocatalysis in aqueous solution: assessing the contribution of thermal effects and evaluating the role of photogenerated ROS. *Nanoscale* 14, 11612–11618
69. Geng, Z. *et al.* (2023) Achieving maximum overall light enhancement in plasmonic catalysis by combining thermal and non-thermal effects. *Nat. Catal.* 6, 1241–1247
70. Sivan, Y. *et al.* (2020) Experimental practices required to isolate thermal effects in plasmonic photo-catalysis: lessons from recent experiments. *OSA Continuum* 3, 483–497
71. Baffou, G. *et al.* (2020) Simple experimental procedures to distinguish photothermal from hot-carrier processes in plasmonics. *Light Sci. Appl.* 9, 108
72. Dubi, Y. *et al.* (2020) Thermal effects - an alternative mechanism for plasmon-assisted photocatalysis. *Chem. Sci.* 11, 5017–5027
73. Kim, Y. *et al.* (2016) Activation energies of plasmonic catalysts. *Nano Lett.* 16, 3399–3407
74. Keller, E.L. and Frontiera, R.R. (2018) Ultrafast nanoscale Raman thermometry proves heating is not a primary mechanism for plasmon-driven photocatalysis. *ACS Nano* 12, 5848–5855
75. Sarhan, R.M. *et al.* (2019) The importance of plasmonic heating for the plasmon-driven photodimerization of 4-nitrothiophenol. *Sci. Rep.* 9, 3060
76. Golubev, A.A. *et al.* (2018) Plasmonic heating plays a dominant role in the plasmon-induced photocatalytic reduction of 4-nitrobenzenethiol. *J. Phys. Chem. C* 122, 5657–5663
77. Koopman, W. *et al.* (2020) Decoding the kinetic limitations of plasmon catalysis: the case of 4-nitrothiophenol dimerization. *Nanoscale* 12, 24411–24418
78. Dubi, Y. and Sivan, Y. (2019) "Hot" electrons in metallic nanostructures-non-thermal carriers or heating? *Light Sci. Appl.* 8, 89
79. Sivan, Y. *et al.* (2019) Assistance of metal nanoparticles in photocatalysis - nothing more than a classical heat source. *Faraday Discuss.* 214, 215–233
80. Hugall, J.T. and Baumberg, J.J. (2015) Demonstrating photoluminescence from Au is electronic inelastic light scattering of a plasmonic metal: the origin of SERS backgrounds. *Nano Lett.* 15, 2600–2604
81. Szczerbinski, J. *et al.* (2018) Plasmon-driven photocatalysis leads to products known from E-beam and X-ray-induced surface chemistry. *Nano Lett.* 18, 6740–6749
82. Baffou, G. (2021) Anti-Stokes thermometry in nanoplasmonics. *ACS Nano* 15, 5785–5792
83. Park, S. *et al.* (2022) Self-referenced SERS thermometry of molecules on a metallic nanostructure. *J. Phys. Chem. C* 126, 451–458
84. Richard-Lacroix, M. and Deckert, V. (2020) Direct molecular-level near-field plasmon and temperature assessment in a single plasmonic hotspot. *Light Sci. Appl.* 9, 35
85. Meng, Q. *et al.* (2024) Local heating and Raman thermometry in a single molecule. *Sci. Adv.* 10, eadl1015
86. Hu, S. *et al.* (2018) Quantifying surface temperature of thermoplasmonic nanostructures. *J. Am. Chem. Soc.* 140, 13680–13686
87. Zhang, Q.F. *et al.* (2021) Hot-hole-induced molecular scissoring: a case study of plasmon-driven decarboxylation of aromatic carboxylates. *J. Phys. Chem. C* 125, 20958–20971

88. Li, P. *et al.* (2023) Nanoscale thermometry of plasmonic structures via Raman shifts in copper phthalocyanine. *J. Phys. Chem. C* 127, 9690–9698
89. Chen, K.X. and Wang, H. (2023) Origin of superlinear power dependence of reaction rates in plasmon-driven photocatalysis: a case study of reductive nitrothiophenol coupling reactions. *Nano Lett.* 23, 2870–2876
90. Sun, J.J. *et al.* (2019) Role of adsorption orientation in surface plasmon-driven coupling reactions studied by tip-enhanced Raman spectroscopy. *J. Phys. Chem. Lett.* 10, 2306–2312
91. Cai, Z.F. *et al.* (2022) Molecular-level insights on reactive arrangement in on-surface photocatalytic coupling reactions using tip-enhanced Raman spectroscopy. *J. Am. Chem. Soc.* 144, 538–546
92. Koopman, W. *et al.* (2021) The role of structural flexibility in plasmon-driven coupling reactions: kinetic limitations in the dimerization of nitro-benzenes. *Adv. Mater. Interfaces* 8, 2101344
93. Love, J.C. *et al.* (2005) Self-assembled monolayers of thiolates on metals as a form of nanotechnology. *Chem. Rev.* 105, 1103–1169
94. Chen, K.X. and Wang, H. (2022) Plasmon-driven oxidative coupling of aniline-derivative adsorbates: a comparative study of para-ethynylaniline and para-mercaptoaniline. *J. Chem. Phys.* 156, 204705
95. Laurentius, L. *et al.* (2011) Diazonium-derived aryl films on gold nanoparticles: evidence for a carbon-gold covalent bond. *ACS Nano* 5, 4219–4227
96. DeJesus, J.F. *et al.* (2018) N-Heterocyclic carbenes as a robust platform for surface-enhanced Raman spectroscopy. *J. Am. Chem. Soc.* 140, 1247–1250
97. Zhang, Y. *et al.* (2017) Observing the overgrowth of a second metal on silver cubic seeds in solution by surface-enhanced Raman scattering. *ACS Nano* 11, 5080–5086
98. Chen, K.X. and Wang, H. (2023) Metal-adsorbate interactions modulate plasmonic reactivity of chemisorbed nitrophenyl derivatives. *J. Phys. Chem. C* 127, 4104–4114
99. Jollans, T. *et al.* (2020) Effective electron temperature measurement using time-resolved anti-Stokes photoluminescence. *J. Phys. Chem. A* 124, 6968–6976
100. Yu, Z.W. and Frontiera, R.R. (2023) Ostensible steady-state molecular cooling with plasmonic gold nanoparticles. *ACS Nano* 17, 4306–4314